Proceedings of the IASS Annual Symposium 2016
"Spatial Structures in the 21st Century"
26–30 September, 2016, Tokyo, Japan
K. Kawaguchi, M. Ohsaki, T. Takeuchi (eds.)

Low-Cost Double Curvature: Geometrical and Structural Potentials of Rectangular, Cold-Bent Glass Construction

Philipp EVERSMANN*, Eike SCHLING[a], André IHDE[b], Christian LOUTER[c]

*ETH Zurich
Zwinglistr.43, 8004 Zurich
eversmann@arch.ethz.ch
[a] TU München
[b] TU München, Pfeifer Seil- und Hebetechnik GmbH Memmingen
[c] TU Delft

Abstract

The realization of doubly curved façades often requires large investments in fabrication equipment and produces additional waste through subtractive fabrication processes and non-reusable molds. In glass construction, elastic bending techniques can be used for small curvatures. This paper continues previous research of the authors on bending rectangular glass elements into irregularly curved panels. First, we analyze the stresses occurring in cold bent glass during assembly, thus defining a particle-spring model which is able to compute approximate stresses in real-time during the bending procedure. In a second step, we compare the structural performance of the bent glass with that of flat panels using FE-analysis. Finally, we illustrate the implementations on multi-panel façade layouts. We analyze the dependencies between curvature, gap-tolerance and panelization. We present a method to minimize gap-tolerances by optimizing the distribution of surface curvature. Our results highlight the structural and geometrical potentials and possible applications for curved glass construction.

Keywords: glass, cold-bending, FE-analysis, particle-spring model, optimization

1. Introduction

In our previous research we have shown how rectangular glass panels can be deformed to approximate double curvature (Eversmann et al. 2016). It would seem logical that a flat panel, after bending, would remain a developable (singly-curved) surface. However, the process of bending glass onto curved frames creates additional strain, which allows some deviation from single into double curvature. In the chapter 2, we show how the bending process functions physically and how it can be simulated using particle-spring modeling. We present a method which allows computing approximate stresses during the simulation in real-time, enabling deformation up to a defined maximum design stress. We proceed by calculating the maximum curvature for a range of surface typologies. In the chapter 3, we compare the structural performance of various curvatures of the surface typologies to that of a flat glass panel. We analyse the maximal deflection, as well as principal and shear stresses on the middle, top and bottom surface of each panel. In chapter 4, we analyze the geometric implications for multi-panel façade layouts. We show geometric possibilities of using a standard 1.0 x 2.0 m panel for doubly-curved design surfaces. We present a simplified method to model large façade layouts, and analyze the dependencies between the curvature of the target surface and the resulting gaps. An optimization method is proposed to simultaneously maximize curvature and minimize gaps. Finally, we suggest application possibilities for future studies.

2. Bending Process and Computational Simulation

In this chapter we will explain the bending process, its computational simulation and deduce a list of criteria, which can be used for subsequent investigations on geometry and structure.

2.1 Methods: Particle-Spring System

The particle-spring model from previous studies was rebuilt in the software Rhino/Grasshopper using the Kangaroo 2 simulator. We implemented the model through custom Python programming in order to calculate stresses resulting from the bending procedure in real time. We were therefore able to bend the panels only as far as the maximum bending stress would allow. The goal of the model was not to replace a proper FE-analysis but to allow the designer to get approximate results on the possible curvatures and surface quality that can be achieved on a design target surface. In the particle-spring system a glass panel is modeled as a series of nodes which are inscribed in a quadrilateral mesh. For each node, or particle, all relationships with its neighbors are then described. For each quad, the neighboring particles are connected by linear springs on which we assigned a constant axial stiffness and initial length. We calculated the stiffness values S of the springs via the formula (1):

$$S = \frac{\text{E (Young's Modulus in (N/mm}^2\text{)} \times \text{A (crosssection in mm}^2\text{)}}{\text{L (length in mm)}} \quad (1)$$

Additionally, we applied a bending stiffness between spring pairs via

$K = E \times I$ where E is the Young's modulus in N/mm^2, and I is the second moment of area in mm^4. (2)

Bending Procedure

In order to bend a flat glass panel to achieve double curvature, forces need to be applied simultaneously on multiple points on each side of the panel. Physically this was achieved in the previous study [1] by a laminated aluminum frame which was bent on a 5-axis, milled wooden frame by simultaneously tightening a predefined set of screws.

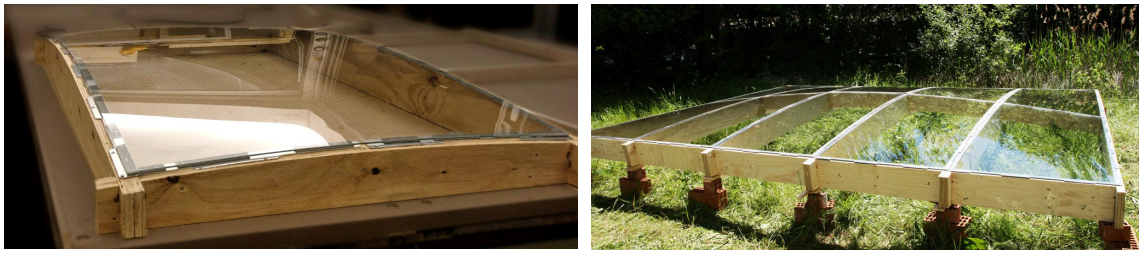

Fig. 1: Physical Prototype and panel assembly from previous study

As shown in figure 2, the frame geometry and force applied by the screws are able to transmit bending forces into the surface of the glass plate. In the simulation, bending is achieved through springs on the panel edges which increase their pulling stiffness until the final geometry is achieved.

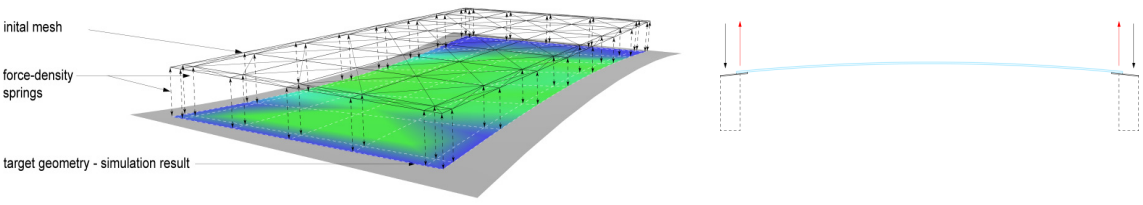

Fig. 2: *Left:* Particle-spring system. *Right:* Bending force vectors

Stress Calculation

For the stress calculation we implemented a custom Python routine for a Kangaroo Goal object to solve the normal stresses and shear stresses. The normal stresses σx , σy are calculated via the change in length of the springs:

$$\sigma x\,,\sigma y = \; S * \gamma \quad \text{where } \gamma = \frac{\Delta L \text{ (new length L}' - \text{inital length L)}}{\text{inital length L}} \tag{3}$$

The shear stresses are calculated via the angle of distortion of the quads:

$$\tau_{xy} = \; G \cdot \gamma_{xy} \quad \text{where G is the shear modulus in } \frac{N}{mm2} \;\; and \;\; \gamma_{xy} = \text{initalAngle} - \text{newAngle in radians} \tag{4}$$

The principal stresses can now be calculated using Mohr's Circle theory [2] via the formula:

$$\sigma 1\,,\sigma 2 = \; \frac{\sigma x + \sigma y}{2} \pm \sqrt{\left(\frac{\sigma x + \sigma y}{2}\right)^2 + \; \tau_{xy}^2} \tag{5}$$

For solving the stresses on the upper and lower surface of the glass plate, the particles are offset in the normal direction of the mesh surface.

Calibration FEM

Various calibration tests were effectuated in order to achieve corresponding results between the particle-spring model and the FE-analysis effectuated in Strand7. Figure 3 shows the corresponding stress distributions of shear and principal stresses.

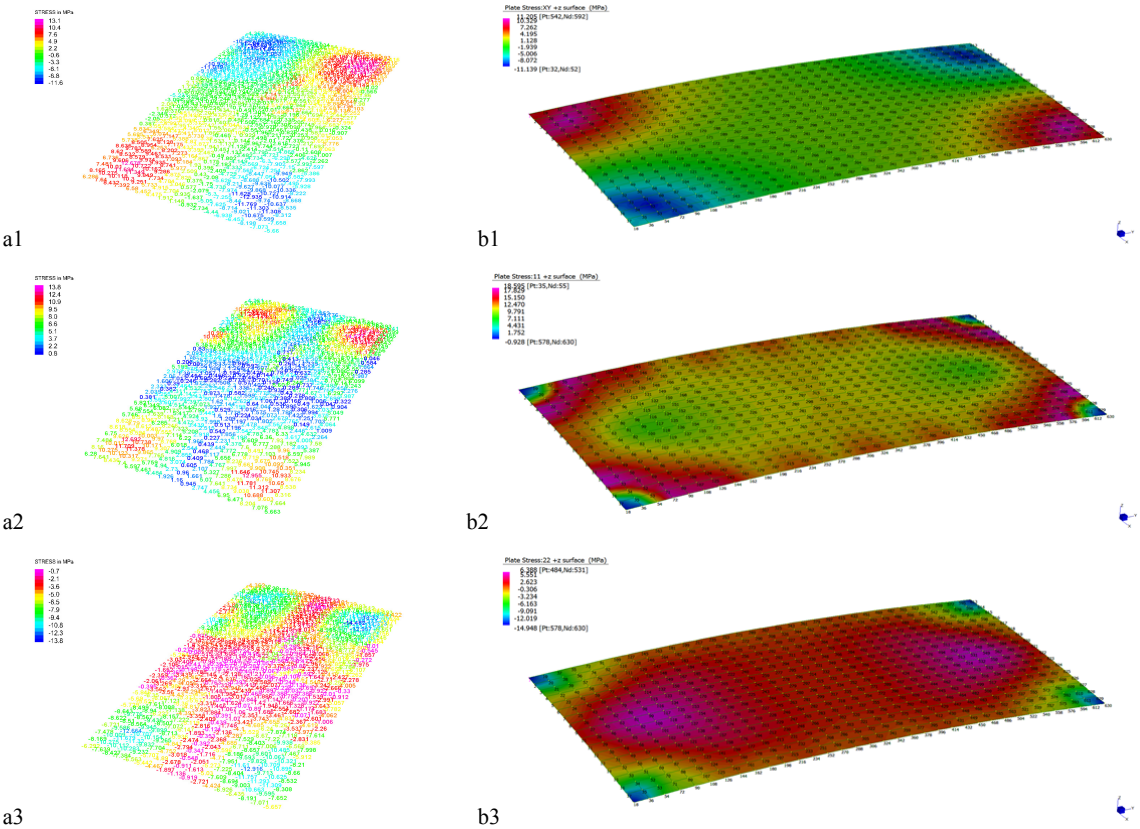

Fig. 3: Calibration of particle-spring model a) and FE-Analysis b), showing the shear stresses in the upper glass layer in the 1st row (a1,b1), the first principal stresses in the second row (a2,b2) and second principal stresses in the third row (a3,b3). Results show a similar distribution of shear stresses, with values varying around 23%. Principal stresses show less detail in the maximum stressed regions and are less precise.

2.2 Results on Various Surface Types

For this study, we applied the particle-spring model on samples of surface types of synclastic and anticlastic typology while trying to maintain a maximum design stress as described by Nicklisch et al. [3] for heat-strengthened glass HSG at 29 N/mm^2. Results were compared with FE-analysis using an automated interchange of model parameters via custom-programmed Excel files. Figures 4-6 show the resulting stress distributions for a 4 mm HSG panel. We also compared the difference to the target surface and analyzed the resulting Gaussian curvature and minimum principal curvature radii of the deformed glass panel.

Target: Hyperparboloid, ruled surface

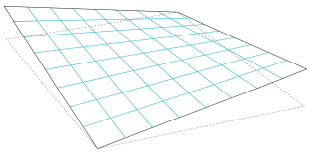

Resulting Geometry:
Min. Principle Curvature (PC) radii : 11.8 m / -11.8 m

		σ1	σ2	τ_{xy}
Z+	max	27.9/ 19.4	-1.5/ 0.6	27.3/ 10.3
	min	1.5/ -0.1	-27.9/ -15.5	-8.5/ 1.7
0	max	14.6/ 18.9	-0.8/ 0.7	9.6/ 3.2
	min	0.8/ -2.2	-14.6/ -8.0	-14.1/ -3.25
Z-	max	21.2/ 19.4	-2.2/ 0.6	-2.2/ -1.7
	min	2.2/ -0.1	-21.3/ -15.6	-21.2/ -10.3

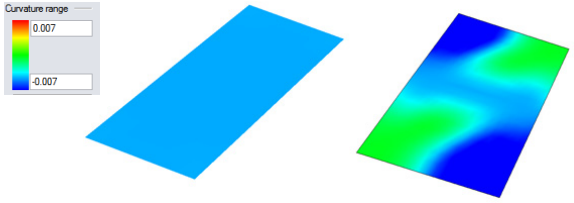

Difference to target surface in mm

Gaussian curvature of target (left) and bent (right) panel

Fig.4: Particle-spring simulation/FE results for bending a rectangular 1.0 x 2.0 m HSG Panel of 4 mm thickness on a target surface of a hyperbolic paraboloid. Results show that the peak stresses occur on the upper surface of the panel close to the corner points. This coincides with the location of maximum Gaussian curvature. The difference to the target surface maximizes in the center of the panel.

Target: Sphere Radius: 8.6m

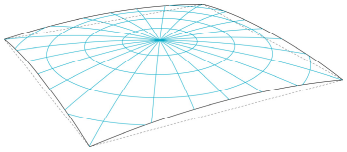

Resulting Geometry:
Min. Principle Curvature (PC) radii : 16.1m/ 24.5m

		σ1	σ2	τ_{xy}
Z+	max	28.4 /29.0	-1.5/8.5	27.0 /15.7
	min	1.6 / -1.3	-28.3/-20.3	-24.9/-15.4
0	max	25.2/ 22.1	-1.4/ 0.9	20.7/15.8
	min	1.4/-6.6	-25.4/-26.4	-24.1/-16.1
Z-	max	24.0/ 29.0	-1.4/ 8.5	22.3/0.8
	min	1.4/-1.3	-24.3/ -20.3	-22.9/-0.8

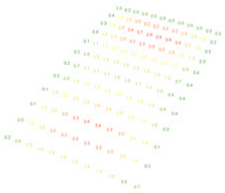

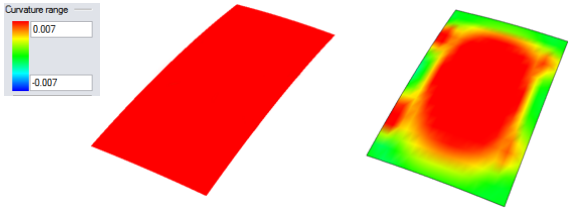

Difference to target surface in mm

Gaussian curvature of target (left) and bent (right) panel

Fig 5: Particle-spring simulation/FE results for bending a rectangular 1.0 x 2.0 m HSG panel of 4 mm thickness on a target surface of a sphere. Results show that the peak stresses occur on the upper surface of the panel close to the corner points. The Gaussian curvature analysis maximizes in the middle and minimizes on the edges. The difference to the target surface maximizes on two clearly separated fields in the middle of the panel.

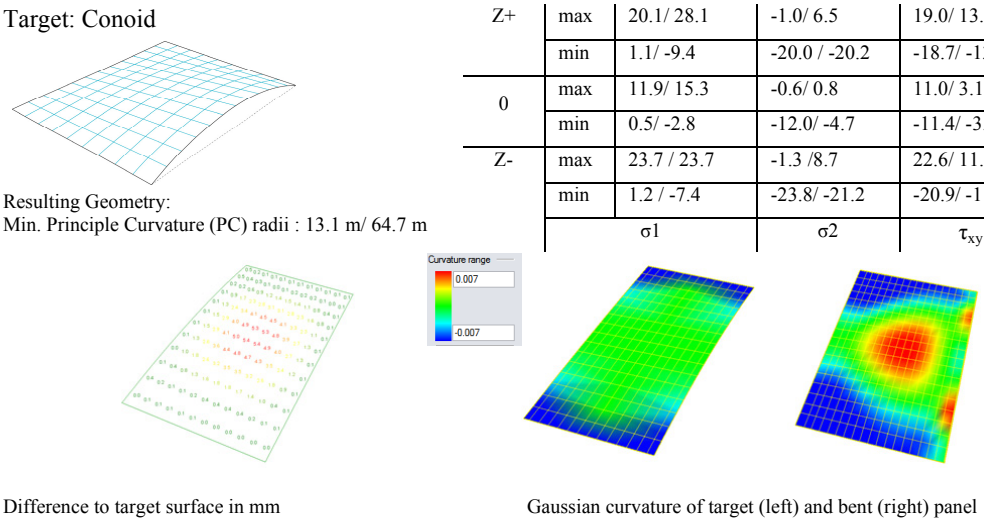

		σ1	σ2	τ_{xy}
Z+	max	20.1/ 28.1	-1.0/ 6.5	19.0/ 13.9
	min	1.1/ -9.4	-20.0 / -20.2	-18.7/ -13.8
0	max	11.9/ 15.3	-0.6/ 0.8	11.0/ 3.1
	min	0.5/ -2.8	-12.0/ -4.7	-11.4/ -3.1
Z-	max	23.7 / 23.7	-1.3 /8.7	22.6/ 11.9
	min	1.2 / -7.4	-23.8/ -21.2	-20.9/ -11.9

Fig. 6: Particle-spring simulation/FE results for bending a rectangular 1.0 x 2.0 m HSG panel of 4 mm thickness on a target surface of a conoid. Results show that the peak stresses occur on the upper and lower surface of the panel close to the two corners of the flat edges. Shear stresses are also considerably high in these regions. This coincides with the area of maximum Gaussian curvature. The difference to the target surface maximizes in the center of the panel.

3. Structural Analysis

In this chapter we analyze the structural performance of bent glass based on the previous construction criteria and geometric investigation. We look at the behavior of a single bent-glass panel in comparison to a flat panel.

3.1 Modelling

For the verification and calibration of the previously described particle-spring model, a method was developed to import the geometry, meshes and support movements into Strand7 via Excel. Before the analysis, the imported movements were applied to a flat glass panel as defined support displacements. For the investigation of the structural behavior of already bent panels, additional surface loads were applied using the stage manager of Strand7. These loads represented climatic loads, such as wind and snow, and were defined to +1kN/m² (representing pressure) and -1kN/m² (suction). The used non-linear-solver with Kirchoff element-theory (material and geometric nonlinearities) is a direct sparse solver with very accurate termination criteria (deflection criteria displacement zero $1x10^{-8}$ m) and maximum defined 1000 iterations. All calculations converged under 50 iteration steps. The results are shown without extrapolation to the nodes to adapt to the discrepancy between the real linear supports and the node-oriented simulation.

			def (m)	z- (MPa)			middle (MPa)			z+ (MPa)		
Surface type	**Load**			**σ1**	**σ2**	**τ**	**σ1**	**σ2**	**τ**	**σ1**	**σ2**	**τ**
Flat	**wind +**	**max**	0.010	10.03	-1.64	10.35	4.35	0.97	1.41	18.84	10.73	10.08
		min	-0.002	-5.32	-17.86	-10.35	-0.44	-6.29	-1.41	-1.47	-9.41	-10.08
	wind -	**max**	0.002	18.84	10.73	10.08	4.35	0.97	1.41	10.03	-1.64	10.35
		min	-0.010	-1.47	-9.41	-10.08	-0.44	-6.29	-1.41	-5.32	-17.86	-10.35
Ruled 1	**bending**	**max**	-0.222	6.23	0.09	-1.59	3.79	0.00	0.80	6.51	0.10	3.98
		min	-0.245	-0.09	-4.99	-4.10	-0.50	-2.12	-0.81	-0.08	-4.77	1.63
	wind +	**max**	0.011	15.92	-0.70	7.01	4.56	0.64	1.31	21.58	9.41	15.81
		min	-0.002	-5.57	-20.99	-13.38	-1.80	-4.18	-1.43	-1.45	-14.94	-6.15
	wind -	**max**	0.002	21.76	9.48	6.47	4.89	0.62	1.45	16.59	-0.04	13.57
		min	-0.011	-1.57	-15.23	-16.18	-1.85	-4.00	-1.41	-5.64	-21.16	-7.22
Ruled 3	**bending**	**max**	-0.140	15.09	0.15	-2.03	11.40	0.02	2.40	14.89	0.13	8.31
		min	-0.190	-0.09	-11.88	-8.31	-1.60	-6.06	-2.45	-0.11	-11.86	2.12
	wind +	**max**	0.014	24.09	1.40	5.57	11.72	0.42	3.65	26.54	9.34	21.85
		min	-0.003	-7.54	-26.41	-16.07	-3.37	-5.75	-2.21	-1.02	-22.09	-5.36
	wind -	**max**	0.003	26.22	9.22	5.02	11.15	0.42	2.15	23.31	0.51	15.97
		min	-0.013	-0.77	-21.46	-21.54	-3.32	-5.48	-3.38	-7.35	-26.33	-5.35

Saddle 1	**bending**	**max**	-0.098	10.18	3.03	3.69	3.10	3.10	0.94	11.76	11.76	2.77
		min	-0.125	-1.01	-6.85	-3.77	-1.14	-1.14	-0.95	-1.81	-1.81	-2.75
	wind +	**max**	0.020	24.77	2.51	9.07	15.43	0.00	3.83	36.20	36.20	13.97
		min	-0.004	-14.88	-38.29	-9.02	-2.31	-8.93	-3.84	6.02	6.02	-14.06
	wind -	**max**	0.001	15.02	8.56	9.10	4.77	12.73	1.77	11.83	11.83	8.81
		min	-0.004	-1.49	-10.81	8.93	-0.62	-8.01	-1.76	-6.50	-6.50	-8.88
Saddle 3	**bending**	**max**	-0.076	30.33	7.77	9.15	9.01	0.05	2.72	23.46	2.20	7.51
		min	-0.131	-4.50	-11.89	-8.77	-2.57	-4.75	-2.71	-5.45	-22.43	-7.39
	wind +	**max**	0.005	23	12.04	8.89	14.38	0.81	3.43	22.98	0.28	8.96
		min	0.001	-7,63	-16.57	-8.75	-4.48	-5.21	-3.43	-5.25	-27.58	-8.91
	wind -	**max**	0.001	23.48	8.35	11.48	14.38	2.17	2.46	21.79	2.94	9.87
		min	-0.002	-2.80	-13.20	-11.35	-4.48	-6.55	-2.47	-6.16	-23.81	-10.11
Conoid 3	**bending**	**max**	-0.091	4.88	0.17	4.18	1.26	0.04	0.36	7.46	0.80	3.54
		min	-0.119	-0.53	-6.07	-4.20	-0.38	-0.53	-0.35	-0.19	-4.65	-3.52
	wind +	**max**	0.007	10.41	-2.63	10.97	5.51	1.10	1.76	13.91	12.33	10.77
		min	-0.002	-6.31	-16.96	-11.00	-0.52	-8.99	-1.76	-1.05	-9.81	-10.75
	wind -	**max**	0.003	26.12	8.35	17.96	8.05	0.24	2.50	22.19	1.94	13.07
		min	-0.014	-1.07	-19.44	-17.98	-2.34	-4.04	-2.51	-6.30	-26.10	13.08
Sphere 1 (r = 12m)	**bending**	**max**	-0.129	15.89	0.75	11.31	0.99	0.55	0.48	18.60	6.39	11.21
		min	-0.172	-5.24	-17.71	-11.36	-0.42	-0.99	-0.48	-0.93	-14.95	-11.14
	wind +	**max**	0.002	13.00	0.89	7,32	4.45	1.53	1.90	15.95	10.15	9.72
		min	-0.001	-7.29	-19.94	-8,62	0.00	-7.49	-1.90	-1.04	-12.80	-9.66
	wind -	**max**	0.001	13.00	0.60	15.52	10.27	0.06	1.73	23.21	4.47	12.53
		min	-0.003	-7.29	-21.89	-15.58	-1.40	-5.37	-1.73	-0.83	-16.95	-12.45

Fig. 7: Excerpts from results of FE-analysis: For each surface typology, three curvature variations for design stress of 29 Mpa with additional wind loads were calculated. The table shows the resulting deflection in m, principal stresses and shear stresses in Mpa on the top surface (z+), middle and bottom surface (z-) of each glass panel. The plates are clamped only vertically. Results show that there are some significantly different values depending on the geometry of the curved panel in comparison to the flat panel. The best performing panel is the ruled (1) surface with a utilization of 74% compared to 65% of the flat panel under wind load. The worst performing is the saddle (1) geometry, with a utilization of 132%.

3.2 Assessment of the Results

As already described in chapter 2.2 and shown in figure 7, the general distribution of stress shows very similar results. At few points the maximum stresses can be higher than in the particle spring-model. This is due to the fact that the particle-spring model operates at a much smaller resolution, meaning that peak stresses might occur on points which are not evaluated. The calculated stress and deflection results for the bent elements show significantly different values compared with the flat panel. The closest geometry is the ruled (1) surface with a utilization of maximum glass stress of 74% referring to a 65% at the flat panel under wind load. The maximum deviation could be found at the saddle (1) geometry. The maximum stress of 36 Mpa (132% utilization) is much higher than for the flat glass panel. As expected, the deviations between flat vs. bent are not dominant. All bent elements show a slightly lower deflection because of increased overall stiffness of the bent panels. This effect is due to the small double curvature of the panels.The calculation results already show maximum stresses close to or locally exceeding the allowable stresses of 29 MPa. As previously mentioned, the bent panels are not supported as a shell should be, meaning that the panel would need to be clamped for horizontal movement as well. Shell-like support for bent glass panels should reduce stresses from additional loads. This must be analyzed and compared with the general rule to support glass panels statically determined to avoid internal stresses due to temperature loads and loads coming from deformations of the superstructure, such as a grid shell or a cable net.

4. Geometric Effects and Surface Design

We have shown a method to bend rectangular glass panels into double curvature. This method allows for fast and low-cost assembly on site. What kind of façade surface can be covered with this method? The following chapter discusses the geometric implications of larger panel layouts, focusing on the use of only one standard panel format to cover doubly-curved design surfaces.

4.1 Façade Panelization with a Single Format

The research field of Architectural Geometry has extensively addressed the problem of paneling freeform surfaces and reducing the number of unique panels. However, there are very few examples in which only one panel format is used.

Research on seamless tessellation with flat panels has provided some strategies to avoid the variation of panel dimensions. Using only one format however, can only be accomplished by either restricting the overall geometry to be developable (singly-curved) or tolerating kinks between panels (Huard, 2014). Alain Lobel has classified such meshes, built exclusively from equilateral triangles (http://www.equilatere.net). In a design process however, the faceted appearance is often not intended. Triangular panels are less material-efficient for both fabrication and construction. Furthermore, the process of discretization into straight elements inevitably shifts complexity to the nodes.

A so-called "semi-discrete" approach suggests the subdivision of a surface using a continuous curve network and curved panels. When looking at built examples of smooth, doubly-curved façade coverings, the following strategies can be distinguished: shape restriction, individual tailoring of panels, positive and negative (overlap) gap tolerance and smoothness tolerance (kink between panels). In the following chapter we will only use gap-tolerance to cover a freeform shape with rectangular glass panels. Section 4.2 will describe a computational method to model large panelizations. Section 4.3 shows the analysis of the geometric dependencies between the curvature of the design surface, the resulting gap between panels and the extent of the panel layout. Section 4.4 illustrates effects related to the paneling grid and the alignment of glass-edges. In the final section 4.5 our method is implemented, to design freeform façades. An optimization method is proposed to simultaneously maximize curvature and minimize gaps.

4.2 Setting up a 3D-Modelling Process

The following investigation is based on the assembly of HSG-glass panels (4 mm) with dimensions of 1.0 x 2.0 m. We previously determined a minimal radius of curvature for the target surface to be 8.6 m. Our test setup is based on the assumption that the edge of a bent glass panel will follow a geodesic line on the target surface. Geodesic lines are defined as the shortest path between two points on a surface. They have no geodesic curvature. This property is achieved by rolling a straight strip onto a surface, as is the case when bending the edges of the rectangular glass panels. Furthermore, we assume that panels will not undergo drastic changes in edge and diagonal length. This provides us with the information to iteratively measure and adjust the geodesic length of any edge. The digital model is controlled by a particle spring system. Four points are projected onto a surface and connected with six geodesic curves; four curves create a quad, and the other two create the diagonals. We then reposition the points on the surface until all curves fulfill the expected length requirements (Fig. 9). The resulting quad will approximate the outline of the bent glass panel with sufficient accuracy.

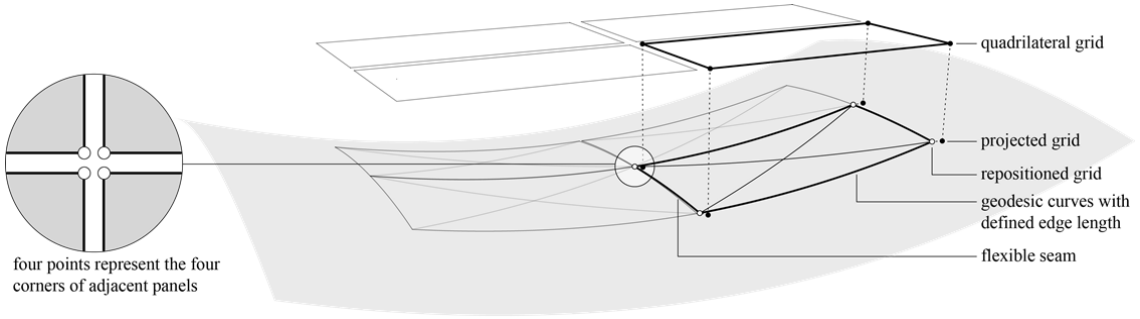

Fig. 9: Modelling process: A quadrilateral point grid is projected onto the target surface. The projected grid is then adjusted to fulfill the expected geodesic-length requirements. Additionally, a seam is simulated by individually modelling each corner of every panel. The resulting four points at each intersection can move independently.

Using this method, we can manipulate any quadrilateral point grid on a surface by adjusting the geodesic distance of one point to its eight neighbors to the expected values of 2.0 x 1.0 m for the edge dimensions, as well as 2.236 m for their diagonal dimensions. This process will yield a homogenous, seamless grid of equidistant panels for any developable (singly-curved) surface, such as flat planes, cylinders or cones. In case of a freeform surface however, the algorithm does not converge fully. It is

impossible for all panels to remain rectangular and congruent, and at the same time seamlessly cover a doubly-curved surface. To counter this, we introduced a flexible seam between the panels. This seam will adjust its width to ensure that the panel-grid can be transformed to the defined dimensions. We do this by creating four points at every intersection in a façade grid; each point represents the corner of one of the adjacent panels. These four points can move apart to allow the edges to fulfill our defined relationship of geodesic lengths.

4.3 Curvature, Layout and Seams

For our analysis this computational setup is applied on a sphere and a hyperbolic paraboloid – two surfaces with homogenous positive and negative Gaussian curvature. Any geometric effect on panelization will be displayed most extremely on these two shapes. We first run the panel-fitting algorithm and then measure the difference in width between smallest and largest seam. We call this value the seam variance (δ).

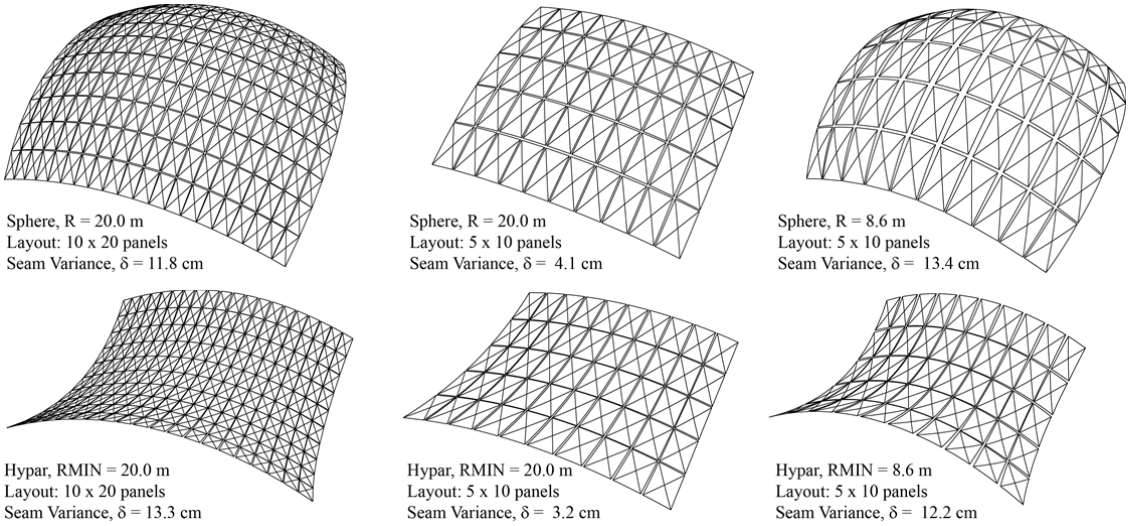

Fig. 10: Two target surfaces: A sphere (*top row*) and a hyperbolic paraboloid (Hypar) (*bottom row*). Each panel has a standard format of 1.0 x 2.0 m. The seam width increases with the greater layout size (*left column*) and smaller curvature radii (*right column*). Synclastic curvature will result in a convex seam; anticlastic curvature causes a concave seam. Seams are more pronounced along the long side of the rectangular panels.

Curvature and layout influence the progression and size of seams throughout the grid (Fig. 10). On synclastic surfaces, the seams follow a convex, banana-like shape. Anticlastic surfaces produce a concave, hour-glass-shaped seam. A smaller curvature radius of the target surface will create a larger seam in the panelization. The layout size also has an increasing effect on the seam's dimensions. Rectangular panels cause wider seams along their long edge.

4.4 Uni-Directional Seams, "Stepping"- and "Bulging" Effect

The orientation of seams can be shifted to only one direction. This property can be useful when designing with a linear substructure. This is achieved by enforcing collinear edges in the opposite direction. It however can trigger a "stepping" effect transversal to the main seam. Fig. 11 shows two panelizations of the same target surface with seams oriented in opposite directions.

As mentioned in section 3.2 the edges of each panel lie on a geodesic curve along the surface. The panel grid however may deviate from a geodesic curve as shown in Fig. 12. Because of this deviation, succeeding glass-edges do not follow a continuous curve. When aiming our view along the panelization grid, we notice the panel edges "bulging" from node to node, creating a cloud-like or

serrated edge. In our example, this effect is most pronounced along the boundary (up to 2 cm) and vanishes towards the center.

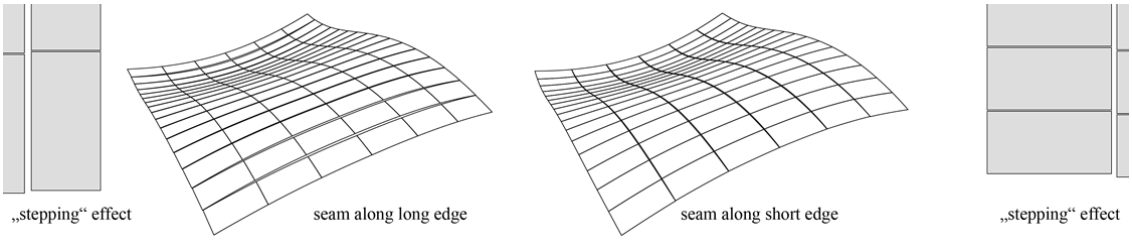

Fig. 11: Freeform surface with uni-directional seams. This can trigger a “stepping” effect transversal to the wider seam.

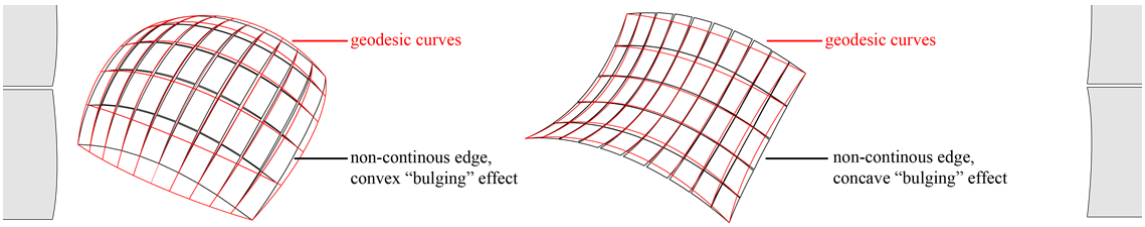

Fig. 12: Spherical and hyperbolic layout with minimal curvature radius 8.6 m. Shown are the resulting pattern of our panel-fitting routine (black) and geodesics connecting the corner vertices (red). When deviating from a geodesic curve, the glass edges do not follow a continuous curve. They “bulge” individually from node to node creating a tolerance of up to 2 cm.

4.5 Freeform Design Using Rectangular Glass Construction

To design an appropriate surface for the use with rectangular, bent glass, we have to avoid surpassing the critical curvature radii. This can easily be done by simultaneously analyzing and manipulating a design surface until no radius violation is detected.

In the following section, we aim to distribute positive and negative curvature evenly across a freeform surface. This will minimize the size of the seams over a large panelization. The setup is based on an optimization loop using a genetic algorithm. A large population of surfaces is generated via control points by randomly varying the Z-value of a point-grid. The following three indicators are then measured at regular intervals across the surface.

$$\text{Fitness: } F = K_{SUM} * (1+K_{PEN}) * L_{RANGE} \quad (6)$$

where $\mathbf{K_{SUM}}$ is the sum of all curvature radii measured on the surface grid, as absolute values, $\mathbf{K_{PEN}}$ is the sum of penalties given for any curvature radius below a minimum value (8.6 m) and $\mathbf{L_{RANGE}}$ is the difference between the longest and the shortest curve along each direction of the surface grid, indicating a homogenous distribution of surface area.

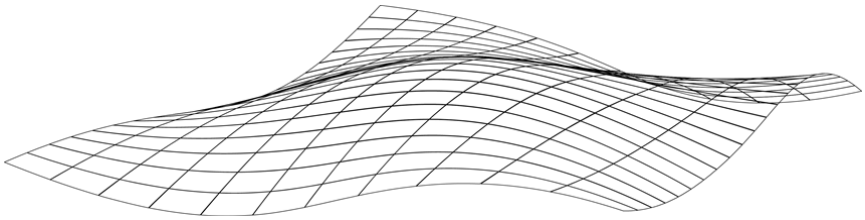

Fig. 13: Optimized freeform surface: Maximizing the overall curvature without violating the minimal radius criteria and minimizing the differences of surface length measured along the panel grid. This results in a maximally curved surface, with low variation of seams: Layout: 11 x 22 panels, $R_{MIN} = 8.61$ m, $\delta = 4.9$ cm

The algorithm evaluates each surface for its fitness F, favoring surfaces with the lowest F-value. Eventually a set of solutions with minimal value F is found. These surfaces have the properties of high

curvature within the bounds of the minimal curvature radii, and a balanced distribution of surface area. They are optimal for the use of curved rectangular panels, as they cause a minimum of seam variations.

5. Conclusion

We have shown that the bending process can be efficiently simulated using a particle-spring model. This modeling technique allows us to bend the panels into as much curvature as allowed within the maximum defined design stresses. This is achieved by calculating and analyzing stresses in real-time. Therefore, any target surface, defined by the architectural designer can be approximated into panels of buildable curvature. We calibrated the modeling technique with the FE-analysis software Strand7 and calculated the maximum Gaussian curvature for surfaces of doubly-ruled, sphere and conoid typology for a given panel of 1.0 x 2.0 m of 4 mm HSG glass. This allowed us to define a minimal bending radius for the subsequent investigation of geometric potentials on multi-panel façade layouts. In our geometric analysis we set up a computational method, which allowed us to quickly simulate large panelization layouts, using only rectangular panels. We analyzed the dependencies of curvature, layout size and seams, and illustrated different effects on the resulting panelization grid. We implemented our modelling method to design and optimize freeform surfaces.

Future investigations might integrate the calculation of external loads in the particle-spring model allowing for multi-criteria optimization. Another research area is the ongoing development of the physical façade detailing of doubly-curved, cold-bent glass construction. The combined behavior of the substructure in connection (stiffening effect) with the bent glass panels will be subject of future research. Future research may investigate the potential of orthogonal nodes in the curvilinear substructure. Further cost efficiency could arise from a careful negotiation of tolerable seam dimensions and tailoring of panels.

Acknowledgements

The physical prototypes were constructed during a Master's elective course at EPF Lausanne held in collaboration between Philipp Eversmann, Paul Ehret, Christian Louter, Manuel Santarsiero and the students Andrea Baraggia, Dominik Baumann, Tomas Odelbo, Agnes Ulrika Charlotta Orstadius, Francesca Rabbiosi, Itai Vander, Robbert Verheij and David Viladomiu Ceballos.

References

[1] Eversmann P., Ihde A., Louter C., "Low cost double curvature – Exploratory computational modelling, FE-analysis and prototyping of cold-bent glass", in *Proceedings of the Challenging Glass 5 Conference,* Belis, Bos & Louter (Eds.), Ghent University, June 2016, 81-92

[2] https://en.wikipedia.org/wiki/Mohr%27s_circle

[3] Nicklisch, F., Thieme, S., Weimar, T., Weller, B.: "Konstruktion und Bemessung Vertikal- und Überkopfverglasungen, Absturzsichere Verglasungen, Begehbare Verglasungen", Glasbau-Praxis: Berechnungshilfen Broschiert (2010) p. 295

[4] Huard M., Eigensatz M. and Bompas P., Planar Panelization with Extreme Repetition, in *Advances In Architectural Geometry 2014*, Block P et al (eds.), Springer, 2014, 256-279

[5] Fildhuth T. and Knippers J., Geometrie und Tragverhalten von doppelt gekrümmten Ganzglasschalen aus kalt verformten Glaslaminaten, in *Stahlbau Spezial 2011 – Glasbau/Glass in Building*, Ernst & Sohn, 2011, 31-44

[6] Bo P., Pottmann H., Wang W. and Wallner J., Circular Arc Structures, in *SIGGRAPH 2011*, ACM 2011, Article No. 101